Numerical Solution of a Hyperbolic System of Conservation Laws with Source Term Arising in a Fluidized Bed Model

I. Christie and G. H. Ganser

Department of Mathematics, West Virginia University,
Morgantown, West Virginia 26506

AND

J. M. Sanz-Serna

Departamento Matemática Aplicada Y Computación, Facultad de Ciencias.
Universidad de Valladolid. Valladolid. Spain

A model of a gas fluidized bed is considered which leads to a hyperbolic system of conservation laws with a source term. The system is solved numerically by a second-order operator splitting technique based on a Roe approximate Riemann solver. Numerical experiments demonstrate the ability of the model to reproduce qualitatively the slugging phenomenon in the case when the bed is subject to a relatively large gas flux   © 1991 Academic Press, Inc

1. Introduction

To fluidize a bed of particles, a flow of gas is forced through the spaces between the particles. If the gas flow is increased, a point is reached where the weight of the particles is first balanced by the upward force of the gas and the bed becomes fluidized (see, for example, Zenz and Othmer [21]). Beyond this state of minimum fluidization, a further increase of the gas velocity frequently leads to other equilibrium states. These are characterized by virtually constant concentration and zero average velocity for the particle phase throughout the bed. With faster gas flow the corresponding equilibrium concentration becomes smaller. This passage through stable equilibrium states continues, as the flow rate is increased, until a critical flow rate is reached when non-uniformities, known as "bubbles" or "slugs," appear in particle concentrations.

By viewing the particles as a continuum, conservation equations can be written for the particle phase, as well as for the gas phase (Drew [3]). With appropriate choices for the constitutive equations, various mathematical models arise for the study of fluidized beds. These models have been analyzed using linear theory to

investigate the onset of slugging (Foscolo and Gibilaro [6], Needham and Merkin [12]). This has shown that with the proper choice of constitutive assumptions, the equilibrium states are initially stable and become unstable at a larger critical gas flow. To determine the fate of the model at a flow rate above this critical velocity, nonlinear analyses have been performed on the equations of motion (Fanucci *et al.* [4, 5], Foscolo and Gibilaro [6], Needham and Merkin [12]).

The models used in nonlinear studies can be distinguished by the presence or exclusion of a particle viscosity term. It has been suggested (Fanucci *et al.* [5], Needham and Merkin [12]) that particle viscosity, no matter how small, is essential for the periodic behaviour corresponding to slugging. In the studies of the hyperbolic models with no particle viscosity, the oscillatory behaviour was guaranteed by analyzing the evolution of periodic initial data (Fanucci *et al.* [4], Foscolo and Gibilaro [6]). Although the appearance of a shock prevented the numerical calculations from proceeding further, it was interpreted as the start of slugging.

The goal of this paper is to demonstrate numerically that a simple hyperbolic model, without particle viscosity, is capable of reproducing the oscillatory slugging behaviour. Moreover, the procedure developed here allows the solution to develop large amplitude shocks and enables us to study their evolution. An analytical study of travelling wave solutions of our system, by Ganser and Lightbourne [7], has verified the existence of this type of solution.

The hyperbolic model has the form of a system of conservation laws with a source term. The numerical algorithm employed is based on known techniques. It uses Strang's second-order splitting [19] to separate the contribution of the source term. The flux terms are integrated by the formally second-order method suggested by Roe [15, 16] with a superbee flux limiter (Sweby [20]) and supplemented by the "entropy fix" of Harten and Hyman [9]. The body force term is dealt with in closed form.

In Section 2 we describe the background of the model. In Section 3 we comment on our choice of numerical algorithm. The most salient features of the code employed are outlined, with special emphasis on the construction of the approximate Jacobian and the difficulties encountered by the occurrence of vacuums. In Section 4 numerical experiments are presented that clearly demonstrate the ability of the model to simulate the slugging phenomenon.

2. DIFFERENTIAL EQUATIONS

In this section we present the system of differential equations to be solved. References for these models are Foscolo and Gibilaro [6], Drew [3], Needham and Merkin [12], and Homsy *et al.* [10]. Since large amplitude solutions are expected, some care is necessary in selecting constitutive equations to capture the correct qualitative behaviour over a wide range of particle concentrations and velocities. The concentration of particles by volume is denoted by α and the velocities of the particle and continuous phases are represented by u and v, respec-

tively. If we assume that each phase is incompressible, the conservation of mass equations are

$$\alpha_t + (\alpha u)_x = 0, \tag{2.1}$$

$$(1 - \alpha)_t + [(1 - \alpha)v]_x = 0, \tag{2.2}$$

where x is the coordinate along the vertical axis and t is time. From (2.1) and (2.2), the quantity $\alpha u + (1 - \alpha)v$ is x-independent. It is clear that this quantity represents the total volumetric flux j through the bed, which here is assumed to be a constant. Therefore, v may be expressed as the following function of u and α:

$$v = (j - \alpha u)/(1 - \alpha). \tag{2.3}$$

The conservation of momentum in the particle phase is given by

$$\alpha \rho(u_t + u u_x) = -\alpha p_x + (p_i - p)\alpha_x - \alpha \rho g + B(v - u), \tag{2.4}$$

where ρ is the particle density, p is the pressure in the particle phase, p_i is the pressure at the interface, g is the acceleration of gravity, and $B = B(\alpha)$ is the drag coefficient. Friction between the particle phase and the tube wall has not been accounted for in (2.4). Friction factors are available for very small particle concentrations because of the importance of pneumatic conveyance of solid particles. However, there appear to be no suitable particle–wall friction factors for the larger particle concentrations occurring in the present application (Baker and Geldart [2]). Although this implies that a meaningful quantitative comparison between theory and experiment is not possible, it should not significantly affect the qualitative behaviour, since the particle–wall friction factor would not contain any gradients. As in Needham and Merkin [12] and Fanucci et al. [5], we are using a linear drag law, primarily due to its analytical simplicity. The simplicity was especially useful in the analysis by Ganser and Lightbourne [7]. A comparison of the analysis in [7] and the numerical computations produced by the algorithm developed here will form part of our future work. It seems likely that the use of more realistic drag laws such as given by Foscolo and Gibilaro [6] will not change the qualitative behaviour.

Since the density of the gas is much smaller than ρ (Needham and Merkin [12]), the gas momentum equation can be written as the equilibrium between friction and gradient of pressure,

$$-(1 - \alpha)(p_g)_x + B(u - v) = 0, \tag{2.5}$$

where p_g is the pressure in the gas.

It is further assumed that in (2.4) $p_i = p_g$ and $p = p_g + \beta$, where $\beta = \beta(\alpha)$ is a non-negative function of α. Therefore, the pressure in the dispersed phase is larger than the pressure in the continuous phase, and this excess is a function of particle

concentration. The motivation for these assumptions is discussed in Homsy *et al.* [10] and Drew [3].

With these simplifications, (2.5) can be used to eliminate p from (2.4) and to arrive at the equation

$$\alpha\rho(u_t + uu_x) = -(\alpha\beta)_x - \alpha\rho g + (1-\alpha)^{-1} B(v-u).$$

Now, considering (2.3), we obtain

$$\alpha\rho(u_t + uu_x) = -(\alpha\beta)_x - \alpha\rho g + (1-\alpha)^{-2} B(j-u),$$

which can be combined with (2.1) to obtain the conservation form to be used for numerical purposes (cf. Lax and Wendroff [11]),

$$(\alpha u)_t + \left(\alpha u^2 + \frac{1}{\rho}\alpha\beta\right)_x = -\alpha g + \rho^{-1}(1-\alpha)^{-2} B(j-u). \tag{2.6}$$

The differential relations (2.1), (2.6), along with the functions $B = B(\alpha)$, $\beta = \beta(\alpha)$, provide a complete system of equations for the determination of α and u (Needham and Merkin [12]).

We now discuss the functions $B(\alpha)$ and $\beta(\alpha)$. A simple form for the drag coefficient B is (Anderson and Jackson [1], Needham and Merkin [12])

$$B(\alpha) = K\alpha(1-\alpha)^{2-n}, \tag{2.7}$$

where K denotes a constant related to the particle size and gas viscosity and n is a constant with typical values of 3 or 4. Other forms for $B(\alpha)$ can also be chosen (Fanucci *et al.* [5]). In a qualitative theory, Ganser and Lightbourne [7] show that the common properties of these functions are best put in terms of the related function

$$H(\alpha) = \frac{-\alpha^2(1-\alpha)^2 \rho g}{B(\alpha)},$$

where $H(\alpha)$ has the following properties:

   (i) $H(0) = 0$, $H'(0) = -v_\infty$, where v_∞ is the terminal velocity for isolated falling particles.

   (ii) $H(1) = 0$, $H'(1) \geqslant 0$.

   (iii)   There exists $0 < \alpha_I < 1$ such that

$$H''(\alpha) > 0 \qquad \text{for} \quad 0 < \alpha < \alpha_I$$

$$H''(\alpha_I) = 0$$

$$H''(\alpha) < 0 \qquad \text{for} \quad \alpha_I < \alpha < 1.$$

For our numerical calculations, the form (2.7) will be used. From property (i) we have that $K = g\rho/v_\infty$.

The constant solutions α, u of (2.1), (2.6) satisfy

$$-\alpha g + \rho^{-1}(1-\alpha)^{-2} B(\alpha)(j-u) = 0$$

or

$$u = j - v_\infty(1-\alpha)^n. \tag{2.8}$$

Equation (2.8) shows that the concentration of particles α_0, which is at equilibrium with $u = 0$, satisfies

$$j = v_\infty(1-\alpha_0)^n. \tag{2.9}$$

Observe that, increasing j (i.e., turning up the inflowing gas) leads to a smaller value of α_0 for linearly stable α_0 states (see (2.12) below). These relations make it possible to specify α_0, v_∞ as parameters in the model, in lieu of j and K. This concludes our discussion of the coefficient B.

To understand the role of the particle phase pressure $\rho^{-1}\alpha\beta$ it is useful to consider an analogy. The non-homogeneous system of conservation laws (2.1) and (2.6) coincides, from a mathematical point of view, with the Euler equations for an isentropic gas flow, subject to volumetric forces. Here α, u, $\rho^{-1}\alpha\beta$ play, respectively, the role of density, velocity, and pressure in the Euler equations. This interpretation makes it clear that for (2.1), (2.6) the characteristic velocities are $u \pm c$, with c equal to the pressure wave speed

$$c^2 = (d/d\alpha)(\rho^{-1}\alpha\beta). \tag{2.10}$$

The choice for the particle phase pressure $\rho^{-1}\alpha\beta$ is determined by the need to model the behaviour of the bed over a wide range of particle concentrations and the desire to study beds which display slugging in its purest form. The type of slugging we have been discussing is characterized by alternating regimes of dense and dilute concentrations of particles separated by horizontal interfaces through which particles rain evenly. This type of behaviour is widely observed in beds of small diameter containing large and very dense particles (Baker and Geldart [2]). Moreover, these systems tend to become unstable almost immediately after the point of minimum fluidization.

To model this behaviour, we have chosen

$$c(\alpha) = s\alpha/(\alpha_p - \alpha), \tag{2.11}$$

with $s > 0$, $0 < \alpha_p < 1$ constants; α_p, the packing concentration, sets an upper limit for α. For large particles, α_p also corresponds to the equilibrium concentration in the bed at minimum fluidization. The α in the numerator guarantees that in the

limit as $\alpha \to 0^+$, (2.6) reduces to the momentum equation for an isolated particle unless $\alpha_x = \infty$. This choice for $c(\alpha)$ is qualitatively similar to the models discussed in Drew [3] and will allow us to approach the incompressible model as $s \to 0^+$. Integration with respect to α in (2.10) determines the function β.

A linearized stability analysis (Needham and Merkin [12]) shows that the constant solution $\alpha = \alpha_0$, $u = 0$ referred to above is stable under the condition

$$(c(\alpha_0)/v_\infty)^2 > n^2 (1 - \alpha_0)^{2n-2} \alpha_0^2.$$

Taking (2.11) into account, the stability requirement becomes

$$\alpha_0 > \alpha_{0u}, \qquad (2.12)$$

where α_{0u} is given by

$$s = n(1 - \alpha_{0u})^{n-1} (\alpha_p - \alpha_{0u}) v_\infty. \qquad (2.13)$$

Since an increase in volumetric flux j implies a decrease in the equilibrium concentration α_0 (cf. (2.9)), the condition (2.12) establishes that, as expected, turning the gas up will endanger the stability of the bed. Note that $s \to 0^+$ corresponds to $\alpha_{0u} \to \alpha_p^-$, thus giving the desired behaviour of a bed which becomes unstable almost immediately after minimum fluidization.

The system (2.1), (2.6) will be solved numerically subject to initial conditions for α and αu and reflecting boundary conditions

$$u = 0, \qquad x = x_L, x_R. \qquad (2.14)$$

These correspond physically to perforated plates preventing the flow of particles.

Before we close this section, it is expedient to seek steady state solutions of (2.1), (2.6), (2.14). Clearly these are given by $u = 0$, along with a solution $\alpha = \alpha(x)$ of the ODE

$$(\rho^{-1}\alpha\beta)_x = -\alpha g + \rho^{-1}(1 - \alpha)^{-2} Bj,$$

i.e., (cf. (2.10))

$$c^2(\alpha)\alpha_x = -\alpha g + \rho^{-1}(1 - \alpha)^{-2} Bj. \qquad (2.15)$$

A typical steady state $\alpha = \alpha(x)$ (uniform fluidization) has been graphed in Fig. 1. Here, with appropriate units, we choose $x_L = 0$, $x_R = 0.5$, $\rho = 1$, $g = 1$, $v_\infty = 1$, $n = 3.5$, $\alpha_p = 0.6$, and $\alpha_0 = 0.55$. The constant s is computed according to (2.13) with $\alpha_{0u} = 0.55$. Note that, following mathematical conventions, we have drawn the x-axis horizontally, even though here x corresponds physically to the vertical coordinate along the bed. Thus, in the situation of Fig. 1, the fluidized particles occupy the bottom of the bed up to a height of approximately $x_{max} = 0.15$. Above this height the concentration is zero. More generally, for the time-dependent problem
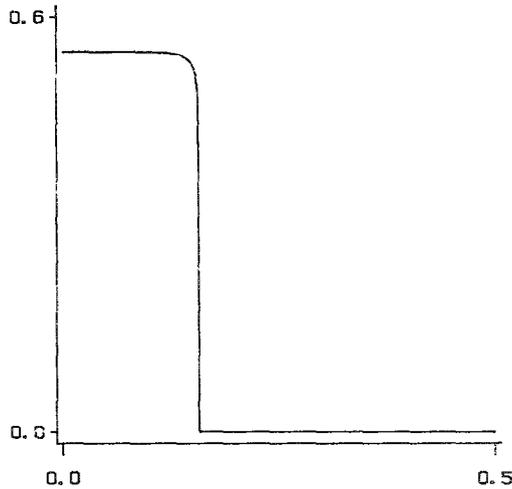
FIG. 1. A typical steady state $\alpha = \alpha(x)$ (uniform fluidization).

(2.1), (2.6), (2.14), it is possible that, at any given time $t > 0$, x-intervals with $\alpha = 0$ (no particles) coexist with x-intervals where $\alpha > 0$. At the boundary between an $\alpha > 0$ and an $\alpha = 0$ region, the function α must be continuous: a discontinuity in concentration would imply a discontinuity in the pressure-like magnitude $\rho^{-1}\alpha\beta$ that is not compatible with the conservation of particle momentum.

Returning to the steady state in Fig. 1, it is interesting to observe that at the foot of the curve we have $\alpha_x = \infty$, in agreement with $c(\alpha = 0) = 0$ in (2.10), (2.15). Also note that, except for a boundary layer, the solution virtually coincides with the equilibrium concentration α_0 associated with the current total volumetric flux j. As observed earlier, a larger value of j corresponds to a smaller value of α_0 and, therefore, to a steady solution where the particles would reach a larger height x_{max} in the bed.

3. NUMERICAL METHOD

The literature on hyperbolic problems has grown enormously in recent years and many numerical methods are now available. Our aim in this paper is to determine the behaviour of the solutions of (2.1), (2.6). A detailed comparison of the merits of several possible algorithms is not our goal and not within the scope of the paper. We shall, therefore, limit ourselves to a description of the algorithm actually used to produce the numerical results presented in the next section. However, some remarks concerning the use of alternative schemes will be given at the end of this section.

The system (2.1), (2.6) being solved is of the form

$$\begin{bmatrix} \alpha \\ m \end{bmatrix}_t + \begin{bmatrix} m \\ \alpha u^2 + F(\alpha) \end{bmatrix}_x = \begin{bmatrix} 0 \\ b(\alpha, m) \end{bmatrix}, \qquad (3.1)$$

where $m = \alpha u$. Note that we have written αu^2 rather than m^2/α as the latter expression is not defined when $\alpha = 0$.

Following Sod [18], we solve (3.1) by operator splitting taking separately into account the flux term $[m, \alpha u^2 + F(\alpha)]_x^T$ and the body force term $[0, b(\alpha, m)]^T$. Sod's approach involved a low-order random choice method for the flux term. Since the fluxes here will ultimately be approximated to second-order accuracy, we employ the well-known, second-order time-splitting due to Strang [19], rather than the simple time-splitting used by Sod [18]. In the present approach, the advancement of the solution over a time interval of length Δt involves taking successively a step of length $\Delta t/2$ with the body force term, a step of length Δt with the flux term, and a final $\Delta t/2$ step with the body force.

For the fractional step corresponding to the system

$$\begin{bmatrix} \alpha \\ m \end{bmatrix}_t + \begin{bmatrix} m \\ \alpha u^2 + F(\alpha) \end{bmatrix}_x = \begin{bmatrix} 0 \\ 0 \end{bmatrix}, \qquad (3.2)$$

we have employed Roe's linearized Riemann solver [14]. For a Riemann problem with given left and right variables $\alpha_L > 0$, m_L and $\alpha_R > 0$, m_R, we first compute the corresponding velocities

$$u_L = m_L/\alpha_L, \qquad u_R = m_R/\alpha_R \qquad (3.3)$$

and then find an approximate Jacobian J that satisfies

$$J \begin{bmatrix} \alpha_R - \alpha_L \\ m_R - m_L \end{bmatrix} = \begin{bmatrix} m_R - m_L \\ \alpha_R u_R^2 + F_R - \alpha_L u_L^2 - F_L \end{bmatrix}. \qquad (3.4)$$

The first row in (3.4) implies that J is of the form

$$J = \begin{bmatrix} 0 & 1 \\ j_{21} & j_{22} \end{bmatrix}.$$

On computing the characteristic equation $\det(J - \lambda I) = 0$, it is found that j_{21}, j_{22} are related to the eigenvalues λ_1, λ_2 of J by

$$j_{22} = \lambda_1 + \lambda_2, \qquad j_{21} = -\lambda_1 \lambda_2$$

so that J is determined by its eigenvalues. As in Roe [14] and Glaister [8], we choose

$$\lambda_1 = \bar{u} - \bar{c}, \qquad \lambda_2 = \bar{u} + \bar{c}, \qquad (3.5)$$

where $\bar{u}$ is the average velocity

$$\bar{u} = \frac{\sqrt{\alpha_R}\, u_R + \sqrt{\alpha_L}\, u_L}{\sqrt{\alpha_R} + \sqrt{\alpha_L}} \tag{3.6}$$

and $\bar{c}$ is an approximate pressure wave speed. On taking these expressions to the second row of (3.4) we find, cf. (2.10)

$$\bar{c}^2 = (F_R - F_L)/(\alpha_R - \alpha_L). \tag{3.7}$$

For numerical purposes, formula (3.7) should be replaced by

$$\bar{c}^2 = dF/d\alpha, \qquad \text{at} \quad \alpha = (\alpha_R + \alpha_L)/2$$

whenever α_L and α_R are close.

Other choices of an approximate Jacobian J satisfying (3.4) would have been possible. An example is given by selecting λ_1, λ_2 as

$$\frac{u_R + u_L}{2} \pm \sqrt{\left(\frac{u_R - u_L}{2}\right)^2 + \frac{F_R - F_L}{\alpha_R - \alpha_L}}. \tag{3.8}$$

So far the Riemann problem being solved was assumed to satisfy $\alpha_L > 0$, $\alpha_R > 0$. As discussed in the previous section, regions with zero concentration are likely to be found and we are therefore interested in solving Riemann problems where either α_L or α_R is zero. Assume that $\alpha_L = 0$, $\alpha_R > 0$. Then, by consistency, $m_L = 0$. In (3.3) u_L is undetermined, in agreement with the fact that the case of zero concentration corresponds physically to a number of isolated particles which may be moving at any speed. However, note that even though u_L is undetermined, the averages $\bar{u}$, $\bar{c}$ in (3.6)–(3.7) have well-defined values $\bar{u} = u_R$, $\bar{c}^2 = F_R/\alpha_R$. Therefore, the construction of J, when either α_L or α_R is zero, can be done by using the same formulas (3.5)–(3.7) as in the case $\alpha_L > 0$, $\alpha_R > 0$. Finally, a Riemann problem with $\alpha_L = \alpha_R = 0$ should have, by consistency, $m_L = m_R = 0$ and therefore leads to a solution $\alpha \equiv 0$, $m \equiv 0$. Note that if we had used the alternative Jacobian in (3.8), we would have found $\lambda_{1,2}$ undetermined when either $\alpha_L = 0$ or $\alpha_R = 0$. The approximate Jacobian in (3.5)–(3.7) can be used to construct first- and second-order accurate schemes for (3.2), as suggested by Roe [15, 16].

The interval $[x_L, x_R]$ is subdivided into N cells of equal length $\Delta x = (x_R - x_L)/N$ and the solution (α, m) is assumed to have a constant value α_i, m_i in the cell $[x_{i-1}, x_i]$, $i = 1, 2, ..., N$; $x_i = x_L + i\, \Delta x$, $i = 0, 1, ..., N$. In the first-order method, the solution is updated as follows. At a cell interface x_i, $i = 1, 2, ..., N-1$, the difference

$$\begin{bmatrix} \Delta_1 \\ \Delta_2 \end{bmatrix} = \begin{bmatrix} \alpha_{i+1} - \alpha_i \\ m_{i+1} - m_i \end{bmatrix}$$

is projected onto the eigenvectors $\underline{r}_1 = [1, \lambda_1]^{\mathrm{T}}$, $\underline{r}_2 = [1, \lambda_2]^{\mathrm{T}}$ of $J(\alpha_i, m_i, \alpha_{i+1}, m_{i+1})$ to find the wave strengths γ_1, γ_2. The corresponding formulas are

$$\gamma_1 = (\lambda_2 \Delta_1 - \Delta_2)/(\lambda_2 - \lambda_1)$$
$$\gamma_2 = (-\lambda_1 \Delta_1 + \Delta_2)/(\lambda_2 - \lambda_1). \tag{3.9}$$

The correction vectors

$$-(\Delta t/\Delta x) \lambda_j \gamma_j \underline{r}_j, \qquad j = 1, 2, \tag{3.10}$$

are used to update either $[\alpha_i, m_i]^{\mathrm{T}}$ or $[\alpha_{i+1}, m_{i+1}]^{\mathrm{T}}$ in an upwind fashion; i.e., if λ_j is positive (negative) then (3.10) is added to $[\alpha_{i+1}, m_{i+1}]^{\mathrm{T}}$ ($[\alpha_i, m_i]^{\mathrm{T}}$).

The previous formulas are meaningful even in cases where either α_i or α_{i+1} is zero. At a cell interface x_i where both α_i, α_{i+1} are zero, the computation of λ_1, λ_2, γ_1, γ_2 is omitted and the corrections (3.10) are replaced by the zero vector.

In practice, the condition $\alpha = 0$ should be replaced by a condition $\alpha \leqslant \text{THRES}$, where THRES is a small value such that, for $\alpha > \text{THRES}$, the pressure wave speed $\bar{c}$ is large enough for the eigenvalues $\lambda_{1,2} = \bar{u} \pm \bar{c}$ to be sufficiently different for the denominators in (3.9) to cause no problem. (Note that, as $\alpha \to 0^+$ the eigenvectors $[1, u + c(\alpha)]^{\mathrm{T}}$, $[1, u - c(\alpha)]^{\mathrm{T}}$ of the Jacobian of (3.2) become linearly dependent and in the limit the system is not strictly hyperbolic.)

Our code tests the condition $\alpha_i \leqslant \text{THRES}$, $i = 1, 2, ..., N$ and sets a flag to monitor the locations x_i at which $\alpha_i = \alpha_{i+1} = 0$. At these locations the approximate eigenvalues $\lambda_{1,2}$ and wave strengths $\gamma_{1,2}$ are not computed. Furthermore, whenever $\alpha_i \leqslant \text{THRES}$ we set $m_i = 0$ and $u_i = 0$. In fact a cell with $\alpha_i \leqslant \text{THRES}$ should be regarded as empty and allocated no momentum. If an empty cell becomes occupied at a later stage, it should only have the momentum of the particles entering that cell, rather than the spurious momentum it would have if m_i had not been set equal to zero. The choice $u_i = 0$ at empty cells is immaterial in light of previous discussions: Any other choice of u_i would essentially lead to the same approximate Jacobian. Note that it is not appropriate to set to zero the values of α_i below THRES as this would prevent a cell from turning from empty to occupied through a succession of updates less than THRES.

It is well known that the simple upwind method just described may produce nonphysical shocks and in fact these were encountered here. The literature contains a variety of techniques ("entropy fixes") for avoiding the occurrence of such shocks. In our code we implemented the procedure described in Harten and Hyman [9].

Formal second-order accuracy is obtained following the recipe of Roe [15] whereby fractions of the corrections (3.10) are used to provide an antidiffusive flux. To avoid oscillations, flux limiters are required (Sweby [20]) and our code uses Roe's superbee limiter [17].

The reflecting boundary conditions, for both the first- and second-order methods are implemented in a standard fashion by the addition of extra, mirror-image cells.

For the fractional time steps involving the body force, the values m_i, $i = 1, 2, \ldots, N$ are updated using the ODE

$$dm_i/dt = b(\alpha_i, m_i). \tag{3.11}$$

Since the expression for b is linear in m_i, Eq. (3.11) is integrated in closed form.

Finally, the choice of Δt is discussed. We proceed from t_n to $t_n + \Delta t_n$ with a step length Δt_n computed at the step from t_{n-1} to t_n. After completing a $\Delta t_n/2$ step with the body force, we compute the maximum modulus μ of the eigenvalues of the approximate Jacobians throughout the domain. If $\Delta t_n > (\text{COURANT}) \Delta x/\mu$, where COURANT is a prescribed constant between 0 and 1, then the CFL condition is violated, the step is rejected and reattempted with a new length

$$0.8(\text{COURANT}) \Delta x/\mu. \tag{3.12}$$

When the CFL condition is satisfied, the flux stage and the remaining body force stage are completed and the length Δt_{n+1} of the next step is set equal to (3.12). This completes our description of the algorithm used in the next section.

Alternative algorithms were also implemented. The simple form of the body force makes closed form integration possible when using splitting. For this reason all alternative algorithms employed splitting, either in Strang's form or in the simple form of [18]. For the flux term we considered the extension of the Engquist–Osher scheme described by Osher and Solomon [13] and several random choice methods. In the E-O scheme, the Jacobian is averaged over a path of states joining the states (α_R, m_R), (α_L, m_L). Even when α_R and α_L are both positive, some portions of the connecting paths may lie in the $\alpha < 0$ region of the (α, m)-plane and special provision must be made to cater for such situations. As a result, the algorithm becomes very involved and we abandoned it in favour of Roe's approximate solver. We did not succeed in obtaining good results when using random choice methods. The failure is perhaps due to the splitting nature of the overall algorithm, but further analysis and experimentation would be required to make a definite assessment.

4. NUMERICAL RESULTS

In this section we describe a selection of the numerical experiments we have carried out. There are two types of results given: those validating the numerical algorithm and those illustrating the slug-producing capabilities of the model.

Unless stated otherwise, all of the constants in the model have the values quoted for Fig. 1 (see Section 2). The first set of numerical calculations concerns the homogeneous system (3.2) together with the initial data

$$\alpha(x, 0) = \begin{cases} 0.3 & -0.2 \leqslant x \leqslant 0 \\ 0.55 & 0 < x \leqslant 0.2 \end{cases}$$

$$u(x, 0) = 0, \qquad -0.2 \leqslant x \leqslant 0.2.$$
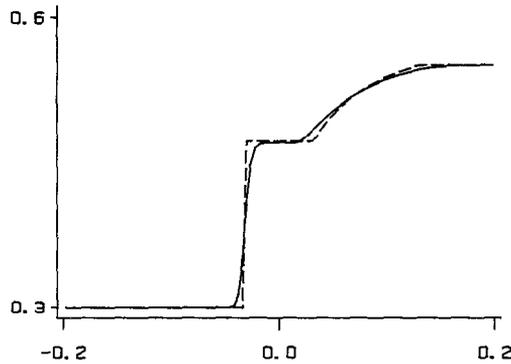
CHRISTIE, GANSER, AND SANZ-SERNA

FIG. 2.   First-order Roe method (continuous line) and exact solution; $t = 0.5$ and $N = 100$.

The exact solution of this Riemann problem, prior to contact with the boundaries, consists of a left-moving shock wave and a right rarefaction wave and this is used to compare the performances of the first- and second-order methods developed in Section 3. The solutions are found, using 100 cells, at $t = 0.5$ (83 time steps for both methods). In Fig. 2 the solution using the first-order method (continuous line) is compared with the exact solution (broken line) and in Fig. 3 the second-order solution is shown. The second-order results are clearly superior to those found by the first-order method in terms of a sharper shock resolution and a rarefaction wave which is indiscernible from the exact form on the scale of Fig. 3.

The second set of numerical experiments is given for the non-homogeneous system (3.1) with a view to investigating the slug-producing capabilities of the model. At $t = 0$ the initial concentration is taken to be the steady state form shown in Fig. 1 and the velocity is zero. As described in Section 2, with the choice $\alpha_0 = \alpha_{0u} = 0.55$, used in the computation of Fig. 1, this profile represents a steady state of the system (3.1). However, our runs had $\alpha_0 = 0.4$, while keeping $\alpha_{0u} = 0.55$, so
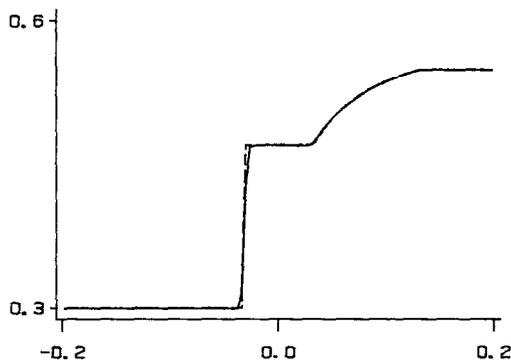

FIG. 3.   Second-order Roe method (continuous line) and exact solution: $t = 0.5$ and $N = 100$.
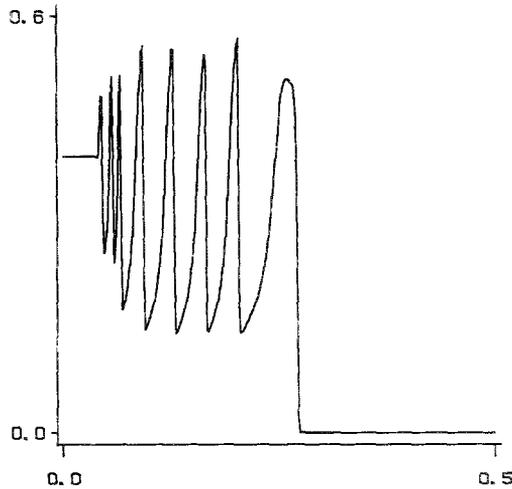
FIG. 4. Second-order Roe method for (3.2), unstable case; $t = 4$ and $N = 400$

that we do not have a steady state any longer. Since, furthermore, (2.12) is violated, instabilities are to be expected. Note that the decrease in α_0 from 0.55 to 0.4 corresponds to an increase in the gas flow. Figure 4 shows the results obtained by the second-order method with 400 cells at $t = 4.0$ (6167 time steps). The presence of a slug-like behaviour is apparent and the method resolves shocks sharply. The position of the right-hand elbow varies as the bed expands and contracts in time. A comparison of these results was made with those obtained using finer grids and this indicated convergence of the scheme.
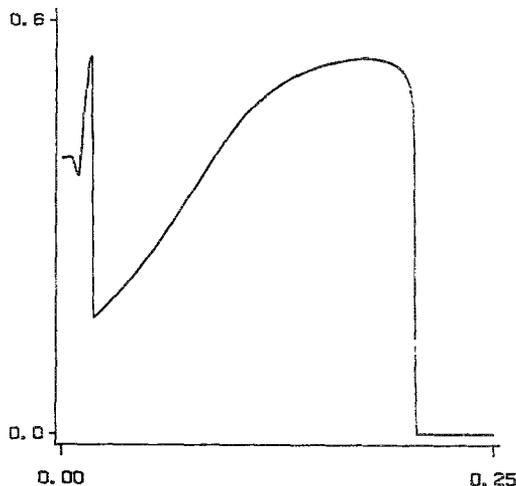

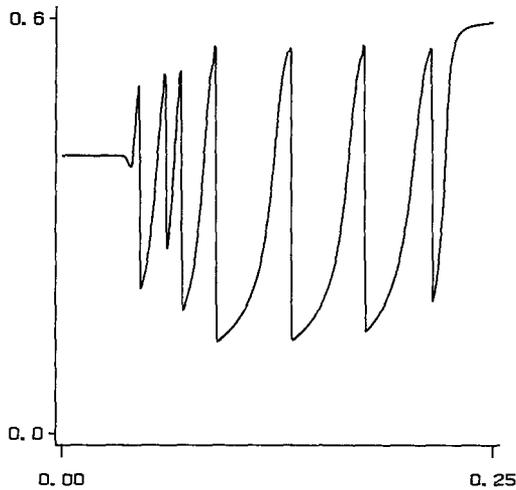FIG. 5. Second-order Roe method for (3.2), unstable case, right boundary, $t = 0.5$, and $N = 400$.

FIG. 6. Second-order Roe method for (3.2), unstable case, right boundary, $t = 4$, and $N = 400$.

In the experiment just described, the boundary at $x = 0.5$ is not active. We therefore decided to run the same experiment with the right boundary located at $x = 0.25$. Although this does not correspond strictly to an actual fluidized bed (which will normally not have a lid), it is presented here as an illustration of the satisfactory performance of the numerical method when both boundaries have an influence. In Fig. 5 the concentration computed by the second-order method at $t = 0.5$ (705 time steps), with 400 cells shows the early evolution of slugs before the particles hit the right boundary. In Fig. 6 the situation at $t = 4$, also with 400 cells, demonstrates the interaction with the boundary. As a result of the collision of particles with the right boundary, values of α are reached close to the packing concentration α_p. The pressure wave speed tends to infinity as α approaches α_p (cf. (2.11)) and, as a consequence, the time step reduced drastically so that 43,320 time steps were required. As in Fig. 4, we have a clear demonstration of the slugging phenomenon.

5. CONCLUSIONS

We have demonstrated that a simple hyperbolic model of a fluidized bed, without particle viscosity, is capable of reproducing the oscillatory behaviour or slugging, for sufficiently high gas velocities. Current work is focused on establishing whether the travelling waves found in the numerical experiments actually correspond to the solution found by Ganser and Lightbourne [7]. If successful, this increased confidence will allow us to explore models which could be quantitatively compared to physical experiments. As discussed in Section 2, the most serious drawback to this

program is the lack of a suitable friction factor between the particles and the wall for high particle concentrations.

Earlier numerical experimentation with hyperbolic models had used the method of characteristics and failed at the onset of shocks. We have used a shock-trapping scheme based on Roe's approximate Riemann solver. While our code is built on known ideas, adjustments had to be made to cater for the presence of vacuums. A Jacobian was employed which could easily cope with vacuums. The Engquist-Osher scheme did not render itself to such a simple treatment of vacuums and random choice methods fared badly on this problem.

REFERENCES

1. T. B. ANDERSON AND R. JACKSON, *Ind. Eng. Chem. Fundam.* 7, 12 (1968).
2. C. G. J. BAKER AND D. GELDART, *Powder Technol.* 19, 177 (1978).
3. D. A. DREW, *Annu. Rev. Fluid. Mech.* 15, 261 (1983).
4. J. B. FANUCCI, N. NESS, AND R.-H. YEN, *J. Fluid Mech.* 94, No. 2, 353 (1979).
5. J. B. FANUCCI, N. NESS, AND R.-H. YEN, *Phys. Fluids* 24 (11), 1944 (1981).
6. P. U. FOSCOLO AND L. G. GIBILARO, *Chem. Eng. Sci.* 42, No. 6, 1489 (1987).
7. G. H. GANSER AND J. LIGHTBOURNE, "Oscillatory travelling waves in a hyperbolic model of a fluidized bed," submitted for publication.
8. P. GLAISTER, *J. Comput. Phys.* 77, 361 (1988).
9. A. HARTEN AND J. M. HYMAN, *J. Comput. Phys.* 50, 235 (1983).
10. G. M. HOMSY, M. M. EL-KAISSY, AND A. DIDWANIA, *Int. J. Multiphase Flow* 6, 305 (1980).
11. P. D. LAX AND B. WENDROFF, *Commun. Pure Appl. Math.* 13, 217 (1960).
12. D. J. NEEDHAM AND J. H. MERKIN, *J. Fluid Mech.* 21, 427 (1983).
13. S. OSHER AND F. SOLOMON, *Math. Comput.* 38, 339 (1982).
14. P. L. ROE, *J. Comput. Phys.* 43, 357 (1981).
15. P. L. ROE, in *Seventh International Conference on Numerical Methods*, edited by W. C. Reynolds and R. W. MacCormack (Springer-Verlag, New York/Berlin, 1981), p. 354.
16. P. L. ROE, in *Numerical Methods for Fluid Dynamics*, edited by K. W. Morton and M. J. Baines (Academic Press, New York, 1982), p. 219.
17. P. L. ROE, in *Lectures in Applied Mathematics*, Vol. 22 (Amer. Math. Soc., Providence, RI, 1985).
18. G. A. SOD, *J. Fluid Mech.* 83, 785 (1977).
19. W. G. STRANG, *SIAM J. Numer. Anal.* 5, 506 (1968).
20. P. K. SWEBY, *SIAM J. Numer. Anal.* 21, 995 (1984).
21. F. A. ZENZ AND D. F. OTHMER, *Fluidization and Fluid-Particle Systems* (Reinhold, New York, 1960).